MEASUREMENT OF BUBBLE PROPERTIES IN A FLUIDIZED BED USING ELECTRICAL CAPACITANCE TOMOGRAPHY

Cornelius Agu*, Lars-André Tokheim, Britt Halvorsen

Department of Process, Energy and Environmental Technology, University College of Southeast Norway, 3918 Porsgrunn, Norway

*Email: *cornelius.e.agu@usn.no*

Abstract – The behaviour of a bubbling fluidized bed can be measured by analyzing appropriate bubble properties. With knowledge of the solids fraction distribution across the bed at any instance, a number of bubble properties can be determined. This study discusses how bubble properties can be obtained using a dual-plane Electrical Capacitance Tomography (ECT). ECT is a non-intrusive sensor consisting of a number of electrodes that measure the distribution of relative permittivity between two phases (for example, solid and gas). Based on the analysis of image data obtained at each plane of the ECT, the criteria for adequate mixing of solids in the bed are established. Since not all bubbles that pass a given plane in the bed may influence its mixing activities, a condition is established for identifying significant bubbles that pass over a plane. For illustration purposes, the flow behaviour of a bed of glass beads with particle size distribution 100-600 μm, is studied and analyzed.

Keywords: Bubble Properties; Fluidized Bed; ECT Sensors; Solid Mixing, Bubbling.

INTRODUCTION

Application of fluidized beds in processes involving chemical reactions requires knowledge about how gas-solids mixing can effectively be achieved. Several techniques have been employed in ascertaining the mixing effect of bubbling beds. Most of the techniques use probes such as pressure and temperature sensors to measure the quality of the fluidized beds (Saxena and Tanjore, 1993; Lin and Wey, 2004). Studies have shown that size, orientation and growth of bubbles are among bubble properties that measure the degree of gas-solids mixing. Bubbles influence the mixing because they carry solid particles in their wakes as they rise up the bed, and the larger a bubble is the larger its wake becomes (Kunii and Levenspiel, 1991). Measurement of pressure fluctuation gives a qualitative indication of passage of bubbles, but not their magnitudes. Recent research on fluidization put focus on the use of tomographs such as X-ray (Bieberle et al., 2010), γ-ray transmission (Werther, 1999) and Electrical Capacitance Tomography (ECT) (Makkawi and Wright, 2004).

In this paper, the use of ECT to measure bubbling fluidized bed properties is described, and results from applying this method are discussed. ECT is a non-intrusive sensor that measures the distribution of relative permittivity between two phases (for example, solid and gas) (Process Tomography, 2009). In addition to its potential to characterize bubble size, shape and 3D orientation, ECT is fast, cheap and flexible to use (Chandrasekera et al., 2015). In fluidized beds, the relative permittivity measurement is directly related to the volume fraction of solids within a section of the bed. Fig. 1 gives the structure of a typical ECT setup with 12 electrodes. To prevent external interferences, the sensor is covered with an outer screen and a guard electrode (Zainal-Mokhtar and Mohamad-Saleh, 2013). The outer screen eliminates the variation in the stray capacitance to earth while the guard electrode protects the sensor from external noise.

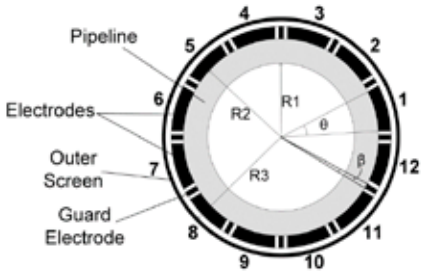

Fig. 1: Structure of an ECT sensor with 12 electrodes. R1 is the inner pipe wall radius, R2 the outer pipe wall radius and R3 the screen wall radius. θ is the electrode angular size and β is the gap within which the guard electrode is 2.5° (Zainal-Mokhtar and Mohamad-Saleh, 2013; Mohamad-Saleh, 2001).

The aim of this paper is to describe how ECT tomographs can be analyzed for determining bubble properties. Such properties include bubble size and shape, bubble frequency, bubble growth and bubble spread. These properties are used to assess the behaviour of fluidized beds at different superficial gas velocities and particle sizes. Particularly in chemical reactions, bubble or gas spread across a bed measures the effectiveness of gas-solids mixing in the reactor (Kunii and Levenspiel, 1991), which is vital for reactor design.

This study is performed using a cold fluidized bed with dual plane ECT sensors. The image data obtained in each plane are processed and analyzed in MATLAB to obtain various bubble properties. In the remaining sections of this paper the bubble properties are described, the experimental techniques adopted for their measurements are explained, and the experimental results are presented and discussed.

BUBBLE PROPERTIES

ECT measures the distribution of relative permittivity between solids and gas in a bubbling bed at a given plane. These permittivity data are used to determine a number of bubble properties, which measure the performance of bubbling beds. The bubble properties include bubble fraction, bubble size, bubble frequency, bubble spread and bubble growth rate. The use of a dual-plane ECT sensor system to measure the solids fraction distribution in a fluidized bed makes it possible to determine the bubble rise velocity when the time it takes a bubble to move between the two planes is known. However, due to frequent coalescence and splitting of bubbles as they move from one plane to another, it is difficult to trace a single bubble (Rautenbach et al., 2011), thus difficult to determine the bubble rise velocity.

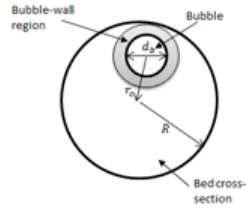

Fig. 2: Illustration of bubble and bubble-wall interaction regions in a bubbling bed.

Bubble diameter

The bubble diameter, d_b in Fig. 2, is the diameter of an equivalent sphere having its projected area the same as the bubble and may be expressed as

$$d_b = \sqrt{\frac{4A_b}{\pi}}, \tag{1}$$

where A_b is the projected area of the bubble. The shape of a bubble can be compared with that of a sphere. The diameter of the sphere d_{bs} is obtained by averaging the lengths of the major and minor axes of an ellipse that has the same normalized second central moments as the bubble (The MathWorks, 1997). The bubble shape factor, φ_b is thus expressed as

$$\varphi_b = \frac{A_b}{A_s}, \tag{2}$$

where $A_s = \frac{1}{4}\pi d_{bs}^2$ is the projected area of the sphere.

Bubble fraction

The bubble fraction describes the fraction of the bed occupied by a bubble at a given instant of time, and it can be expressed as

$$\delta_f = \frac{a_b}{A_t}, \tag{3}$$

where δ_f is the bubble fraction, $a_b(t)$ is the instantaneous projected area of the bubble and A_t is the cross-sectional area of the bed.

Bubble spread

The bubble spread measures the fraction of a region bounded by the wall where the bubbling activities can be felt. The spread could be dynamic as bubbles frequently change orientation (alternately moving towards the wall and towards the center in the bed). The relative frequency of bubble passage near the wall and near the

center of the bed measures the quality of gas-solids mixing in the bed. In this paper, quantities termed bubble location, bubble boundary factor and near-wall to near-center bubble frequency ratio are introduced to quantify the bubble spread.

The factor describing the location of a bubble at any plane is expressed as

$$\delta_l = \frac{(R-r_c)^2}{R^2}, \tag{4}$$

where R is the radius of the plane and r_c is the distance between the center of the bubble and the the center of the plane where the bubble lies as illustrated in Fig. 2. The δ_l value only gives an indication of bubble location relative to the wall of the bed. The location factor lies within $[\delta_l, 1]$. When $\delta_l = \delta_f$, the bubble has contact with the wall, and when $\delta_l = 1$, the bubble lies at the center of the bed plane.

Within the spread region, the ratio of the area surrounding the bubble up to the wall (shaded portion in Fig. 2) to the area of the bubble is termed bubble boundary factor δ_b.

$$\delta_b = \frac{\delta_l}{\delta_f} - 1; \quad \delta_b \in (-1, \infty). \tag{5}$$

In addition to location, the boundary factor indicates relative size of bubbles in a plane. Since $\delta_l > 0$, $\delta_b \to -1$ means that the bubble is very large and $\delta_b \to \infty$ means that the bubble is very small. The value $\delta_b = 0$ indicates that the bubble has a point contact with the wall while $\delta_b < 0$ means that the bubble lies along the wall.

For the purpose of analysis, the bubble properties are usually time-averaged in every plane. For this reason, only the significant bubbles are considered. Since δ_b relates the bubble size to its location from the wall, a value of boundary factor can be used to set a condition for recognizing a significant bubble. In this work, a bubble that has a boundary factor less than 8 is considered significant. The threshold value $\delta_b = 8$ is obtained by assuming that the shortest distance between such a significant bubble and the wall is 3 times its radius.

When there are more than one significant bubbles in a plane, the average distance of the bubbles from the center of the plane can be obtained by taking the second moment of area of all the bubbles about the center:

$$r_c = \left(\frac{\sum(\delta_{fi} r_{ci}^2)}{\sum \delta_{fi}}\right)^{1/2}, \tag{6}$$

where δ_{fi} and r_{ci} are the individual bubble fraction and center distance, respectively.

Bubble spread frequency

Two different bubble spread frequencies are described here: near-wall bubbling frequency and near-center bubbling frequency

The near-wall bubbling frequency, f_w, -is the number of times significant bubbles in the plane moves radially towards the wall of the bed per unit time, while the near-center bubbling frequency, f_c, -describes the number of times significant bubbles in the plane moves toward the center of the plane.

$$f_w = \left[\frac{1}{t_{w,inter}}\right]_{\delta_b \le 0} \tag{7}$$

$$f_c = \left[\frac{1}{t_{c,inter}}\right]_{\delta_b > 0}. \tag{8}$$

The relative value between f_w and f_c indicates the extent of mixing of solid particles in the plane. If $\frac{f_w}{f_c} < 0$, the spread of gas within the plane are more around the center than near the wall, and conversely.

Bubbling frequency

The bubbling frequency is defined as the number of times at least one significant bubble passes through a given plane of a bed in a unit time.

$$f_b = \frac{1}{T_b}, \tag{9}$$

where T_b is the time taken for complete passage of a bubble in the plane. T_b can be obtained as the average period of bubble cycle in the plane (see Fig. 3), as described in Eq. (10).

$$T_b = \frac{1}{n}\sum T_{bi}. \quad (10)$$

Here, n is the number of bubbles that pass through the plane over a period of time and T_{bi} is the individual bubbling period. Higher bubbling frequency indicates a high possibility of gas-solids mixing provided the bubble is large enough to give adequate gas spread in the plane.

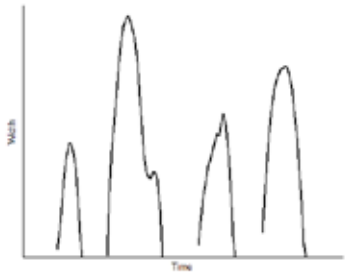

Fig. 3: Variation of projected width of a bubble with time over a plane. Bubbling period is proportional to bubble diameter.

The efficiency of gas-solids mixing due to bubbles can be measured by the volume of bubbles swept in a given time. The rate at which a bubble volume passes over a unit area of a plane (also referred to as bubble flow rate per unit area), can be expressed as

$$v_r = \frac{v_b}{T_b A_t}, \quad (11)$$

where v_r is the bubble flow rate per unit area and v_b is the volume of a bubble. Assuming a spherical bubble, Eq. (11) can be simplified, yielding

$$v_r = \frac{2}{3} f_b \delta_f d_b. \quad (12)$$

A very low value of v_r indicates less possibility of gas-solids mixing due to insufficient gas spread, while a very high value of v_r indicates a poor gas retention time as most of the gas is carried away from the bed by the bubble. With knowledge about the values of v_r, an optimum operating velocity in a bubbling fluidized bed can be established.

EXPERIMENTAL

The setup used in this work consists of a cylindrical column of diameter 10.4 cm and height 1.4 m. The bottom of the column is fitted with a porous plate and an air supply hose. The porous plate ensures even distribution of air in the bed. The measuring equipment is a dual-plane ECT sensor as shown in Fig. 4. The sensors are located at two different positions, 15.7 cm and 28.7 cm above the distributor. Each sensor consists of 12 electrodes, uniformly distributed around the plane circumference. The cross-section of each sensor is divided into 32x32 square pixels, of which 812 lie within the bed. Each pixel holds a normalized permittivity with intensity lying between 0 and 1. When the sensors are energized by the applied voltage, the capacitance between each pair of electrodes is measured and converted into permittivity values according to the relationship $C = SP$ (Process Tomography, 2009). Here, C is an M x 1 capacitance matrix with M = 66 (number of inter-electrode pairs), P is an N x 1 relative permittivity matrix with N = 1024 (number of pixels) and S is an M x N sensor sensitivity matrix. The relative permittivity is evaluated based on the Linear Back Projection algorithm available in the ECT software.

The experiment was performed with glass bead particles of size range 100 – 600 μm having the Sauter mean diameter of 261 μm and minimum fluidization velocity of 0.09 m/s. The fluidizing fluid is compressed air at ambient temperature and superficial velocity of 0.18 m/s ($2U_{mf}$), where U_{mf} is the minimum fluidization velocity. In the experiment, the ECT sensors were first calibrated for the lower permittivity value when the column was empty, and then for the higher permittivity value by filling up with glass particles to a height of 64.0 cm giving the bed aspect ratio $h_0/D = 6.2$. The lower and higher permittivity values defining the range of the equipment are normalized into values 0 and 1, respectively. The normalized relative permittivity ε_r is a measure of volume fraction of solids in the bed. The volume fraction of particles at any point in the plane is

obtained from $\varepsilon = \varepsilon_0 \varepsilon_r$, where ε_0 is the volume fraction of the solid particles in a fixed state. The observed value of ε_0 in this experiment is 0.62.

After the sensor calibration, the bed was fluidized at a superficial air velocity of 0.25 m/s for 2 min, and thereafter the air supply was cut off. This action was to ensure that the particles in the bed were evenly mixed. At a superficial air velocity of 0.18 m/s, the images for solids distribution at each position of the ECT sensors were recorded for 60 s. The image data were captured at a frame frequency of 100 Hz, giving 6000 frames over the 60 s. The recorded image data were exported for analysis in MATLAB and to determine the bubble properties.

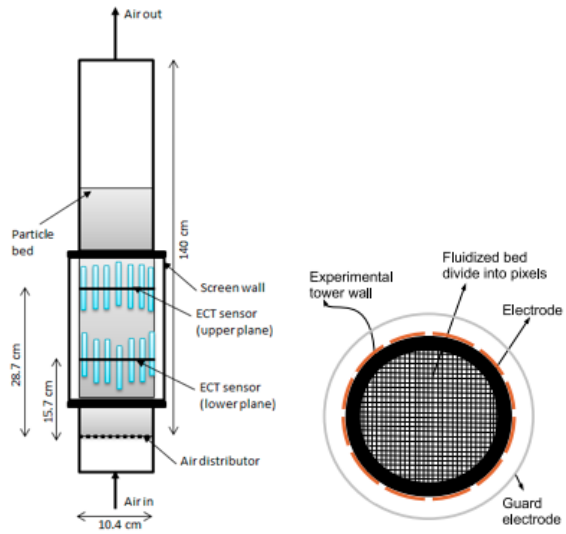

(a) (b)

Fig. 4: (a) Schematic illustration of a cold fluidized bed where two plane ECT sensors are used to measure solids fraction. (b) Cross-section of an ECT sensor divided into 812 pixels.

BUBBLE REGION

A dense fluidized bed is divided into two regions – an emulsion region (of high solids concentration) and a bubble region (of low solids concentration) (Kunii and Levenspiel, 1991). So far, no definite value has been assigned to the bubble-emulsion threshold that marks the boundary of a bubble region. This is because different beds have different bubble rise characteristics due to particle nature and size distribution; also, different equipment units produce different results (Rautenbach et al., 2013).

Different researchers use different values of solids fraction at the bubble threshold. Gidaspow (1994) describes the bubble region as where the solids fraction is less than 0.2. In the work of Rautenbach et al. (2013), the bubble threshold is obtained by trial such that the ECT data are used to estimate the known diameter of a ping-pong ball falling through the bed. Fig. 5 shows the distribution of solids fraction in the bed recorded in the first-30 s at the lower and upper planes of the ECT sensors. In these figures, the blue regions within the bed cross section are evidence that there are bubble passages over the time interval, and as can be seen these regions lie within the solids fraction [0, 0.2]. Hence, bubbles in this paper are defined as regions where the solids fraction is not more than 0.2.

Having identified the bubble threshold, properties such as bubble size (measured by the number of pixels occupied by the bubble) and bubble orientation (measured by the centroid of the bubble) are determined using the image region property toolbox in MATLAB. The actual projected area of a bubble within a plane at any instant is obtained from $A_b = A_t \left(\frac{N_b}{N_{pix}}\right)$, where N_b is the number of pixels occupied by the bubble and $N_{pix} = 812$ is the total number of pixels within the plane.

RESULTS AND DISCUSSION

The information acquired from each of the ECT sensors over 60 s of airflow was analyzed in MATLAB. The results of the experiment and the analysis are shown in Figs. 6 – 7 and Table 1.

Fig. 6(a and b) show the bubble regions in the bed at the 9th s, where the region in white represents the bubble. The bubble shape is compared with that of a sphere represented by the circles.

The time series of the largest bubble that passed each of the planes over 60 s are shown in Fig. 7. The vertical axes represent the projected bubble fraction, while the horizontal axes give the frame time in seconds. These results show that there were a higher number of bubble passages in the lower plane than in the upper plane within a time interval. From the variation of the bubble fraction, it shows that bubbles grow into a more stable size (larger bubble fraction) as they rise in the bed, leading to the more pulsating bubbling recorded at the upper plane.

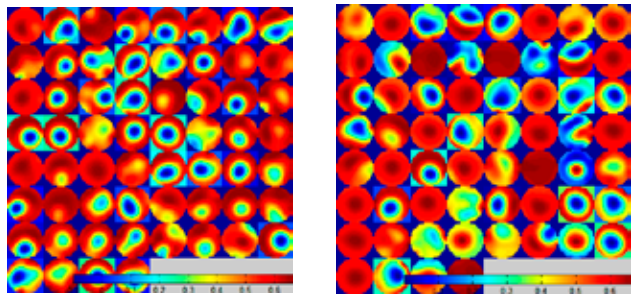

(a) (b)

Fig. 5: Map of solids fraction distribution for the first-30 s taken at 0.5 s interval: (a) lower plane (b) upper plane. Time of sampling increases from left to right and from top to bottom. The superficial air velocity was 0.18 m/s.

(a) (b)

Fig. 6: Behaviour of the fluidized bed in the (a) lower plane and (b) upper plane, at 900th frame showing the region occupied by the actual bubble (white) and region defined by the whole-spherical bubble (bounded by a red circle).

Table 1 shows the time-averaged values of various bubble properties calculated from the solids fraction distribution captured with each of the ECT sensors over 60 s. As shown in Table 1, there are more bubbles rising in the lower plane (frequency 5.97 s^{-1}) than in the upper plane (frequency 3.66 s^{-1}) in a unit time. The difference in the bubbling frequency is associated with different bubble sizes between the two planes: a smaller average bubble diameter 5.04 cm at the lower plane and a larger average bubble diameter 8.00 cm at the upper plane. The bubble size increases due to bubble coalescence and pressure drop along the bed. The smaller bubbles take less time than the larger bubbles to pass over a plane, as shown in Fig. 3, leading to a higher number of bubble passages at the lower plane in a given time. The fraction of the bed cross sectional area occupied by most of the bubbles in each time interval is 19.6% in the lower plane and 43.2% in the upper plane.

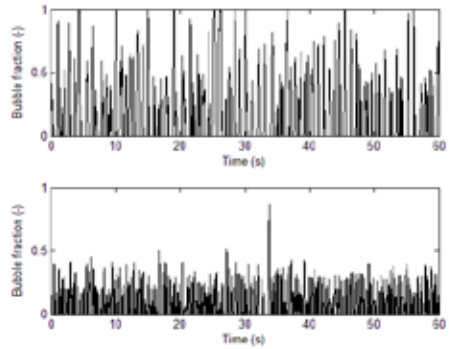

Fig. 7: Projected bubble fraction of the largest bubble as a function of time. Upper plot (upper plane); Lower plot (lower plane).

Table 1: Results: Bubble properties obtained from ECT image data analysis.

Symbols	Lower plane	Upper plane	Units
$\bar{d}_b$	5.04	8.00	cm
$d_{b,max}$	7.85	10.40	cm
φ	0.96	0.79	-
δ_f	0.196	0.432	-
f_b	5.97	3.66	s^{-1}
f_w/f_c	0.055	0.693	-
v_r	3.57	7.14	cm/s

The maximum attainable bubble diameter within 60 s is 7.85 cm at the lower plane and 10.40 cm at the upper plane (the same as the bed diameter). Though there was no fully developed slug in the entire bed, the maximum attainable bubble size at the upper plane indicates a slug flow and with further increase in the superficial gas velocity, the slug will expand to the lower part of the bed (see Fig. 8). The shape factors of 0.96 and 0.79 at the lower and upper planes, respectively, show that a bubble gets less spherical as it grows in size.

The ratio of near-wall bubbling frequency to near-center bubbling frequency in the two planes are less than unity and quite different (0.055 for the lower plane and 0.693 for the upper plane). These values suggest that most of the bubble activities in the lower plane occur near the center of the plane. At the upper plane, the difference in activity is less pronounced - the bubble activity near the center is about twice as high as near the wall. The bubble flow rate per unit area of the bed suggests that the upper plane holds less amount of gas than the lower plane in a unit time. The average of the flow rate across the bed is 5.36 cm/s per unit area.

CONCLUSION

The behaviour of a bubbling fluidized bed was studied by analyzing the bubble properties determined from the measurement of solids fraction distribution using a dual-plane ECT sensor system. With the bubble threshold defined as a region with solids fraction less than 0.2, bubble properties such as size, shape, spread frequency, bubbling frequency and bubble flow rate were determined using the image region property toolbox in MATLAB.

From the bubble spread frequency, it is possible to determine where the bubble activities are concentrated. Knowledge about this aids the design of chemical reactors, for example, for proper heat distribution.

In further works, determination of bubble rise velocity from the ECT image data will be considered. Future work will also be extended to analysis of bubbling bed behaviour from the solids fraction measurement and validation of bubble properties at different superficial gas velocities and bed materials.

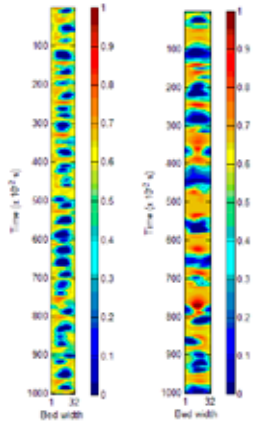

(a) (b)

Fig. 8: Images from the ECT sensors stacked in time for the first-10 s of the flow. Time axis increases from top to bottom. (a) Lower plane: Bubble size is large but less than the bed diameter. (b) Upper plane: Bubble size grows to the size of bed diameter, indicating slugging.

REFERENCES

Bieberle M., Schleicher E., Fischer F., Koch D., Menz H.-J., Mayer H.-G., et al. 2010. Dual-Plane Ultrafast Limited-Angle Electron Beam X-ray Tomography. Flow Measurement and Instrumentation 21(3): 233 – 239.

Chandrasekera T.C, Li Y., Moody D., Schnellmann M.A., Dennis J.S., Holland D.J. 2015. Measurement of Bubble Sizes in Fluidized Beds Using Electrical Capacitance Tomography. Chemical Engineering Science 126: 679 – 687.

Gidaspow D. 1994. Multiphase Flow and Fluidization: Continuum and Kinetics Theory Descriptions, Academic Press Inc., San Diego, California, USA.

Kunii D., Levenspiel O. 1991. Fluidization Engineering, 2nd ed., Butterworth – Heinemann, Washington Street, USA.

Lin C., Wey M.Y. 2004. Statistical and Power Spectral Analysis of Quality of Fluidization for Different Particle Size Distributions at High Temperature. Advanced Powder Technology 15(1): 79 – 96.

Makkawi Y., Wright P. 2004. Electrical Capacitance Tomography for Conventional Fluidized Bed Measurements – Remarks on the Measuring Techniques. Powder Technology, 148: 142 – 157.

Mohamad-Saleh J., Hoyle B.S., Podd F.J.W., Spink D.M. 2001. Direct Process Estimation from Tomography Data Using Artificial Neural Systems. Journal of Electronic Imaging 10(3): 646 – 652.

Process Tomography 2009. Electrical Capacitance Tomography System. Operating Manual Volume 1. Fundamentals of ECT, Process Tomography Ltd.

Rautenbach C., Melaaen M.C., Halvorsen B.M. 2011. Investigating the Influence of Fines in Fluidized Bed Reactors Using 3D ECT Images. In: Mammoli A.A. and Brebbia C.A., editors. Computational Methods in Multiphase Flow VI, Wessex Institute of Technology, WIT – Press, Ashurst Lodge, Ashurst, Southampton SO40 7AA, UK, p141 – 151.

Rautenbach C., Mudde R.F., Yang X., Melaaen M.C., Halvorsen B.M. 2013. A Comparative Study between Electrical Capacitance Tomography and Time-Resolved X-ray Tomography. Flow Measurement and Instrumentation 30: 34 – 44.

Saxena S., Rao N., Tanjore V. 1993. Diagnostic Procedures for Establishing the Quality of Fluidization of Gas-Solid Systems. Experimental Thermal and Fluid Science 3: 56 – 73.

The MathWorks. 1997. Image Processing Toolbox for Use with MATLAB. User's Guide Version 2, The MathWorks Inc.

Werther J. 1999. Measurement Techniques in Fluidized Beds. Powder Technology 102: 15 – 36.

Zainal-Mokhtar K., Mohamad-Saleh J. 2013. An Oil Fraction Neural Sensor Development Using Electrical Capacitance Tomography Sensor Data. Sensors 13(9): 11385 – 11406.